An Experimental Study of Mesler Entrainment on a Surfactant-Covered Interface: The Effect of Drop Shape and Weber Number

B. H. Mills and J. R. Saylor
Dept. of Mechanical Engineering, Clemson University, Clemson, SC 29634

F. Y. Testik
Dept. of Civil Engineering, Clemson University, Clemson, SC 29634

DOI 10.1002/aic.12573
Published online March 22, 2011 in Wiley Online Library (wileyonlinelibrary.com).

Mesler entrainment is the formation of large numbers of small bubbles which occurs when a drop strikes a liquid reservoir at a relatively low velocity. Existing studies of Mesler entrainment have focused almost exclusively on water as the working fluid in a nominally clean state, where even very small levels of contamination can cause significant changes in surface tension that affect the repeatability of the results. Herein water combined with the soluble surfactant Triton X-100 is used as the working fluid in an attempt to stabilize the state of the water surface. Despite this approach, nominally identical drops did not always result in the same bubble formation event. Accordingly, Mesler entrainment was quantified by its frequency of occurrence for drops having the same nominal diameter and impact velocity. This frequency of occurrence was found to be well correlated to both the Weber number and the shape of the drop on impact. © 2011 American Institute of Chemical Engineers *AIChE J,* 58: 46–58, 2012
Keywords: Mesler entrainment, drops, bubbles, surfactants, monolayers

Introduction

When a drop impacts a liquid surface, a range of fluid mechanical phenomena can be observed, including bubble formation, floating or bouncing drops, drop coalescence, and drop splashes (which result in secondary drops that spawn their own drop impact events). Here we are interested in the entrainment of bubbles caused by a drop impact. Bubble entrainment by drop impacts may refer to a number of different types of air entrainment with a wide array of bubble quantities and sizes. The term ‘‘Mesler entrainment’’ is generally accepted to refer to a specific bubble entrainment scenario originally documented by Mesler and co-workers[1–5] where an abundance of micron-scale bubbles is formed during the drop impact that are subsequently propagated into the liquid bulk. This phenomenon occurs at relatively low drop impact velocities; for a water drop having a diameter of order 1 mm, it can be observed when drops are released from heights on the order of 10 mm giving an impact velocity on the order of several hundred mm/s.

Two examples of Mesler entrainment are presented in Figure 1. The image on the left was obtained by Sigler and Mesler,[5] and the one on the right by the present authors. The bubbles appear white on the left and black on the right due to a different orientation of the light source. In both cases the bubbles are located just below where the drop impact crater existed a moment earlier, and a large number of small diameter bubbles are observed, organized in a chandelier-like pattern. In this type of entrainment, the bubbles formed are less than 100 μm in diameter; a lower bound on bubble

Correspondence concerning this article should be addressed to J. R. Saylor at jsaylor@clemson.edu.

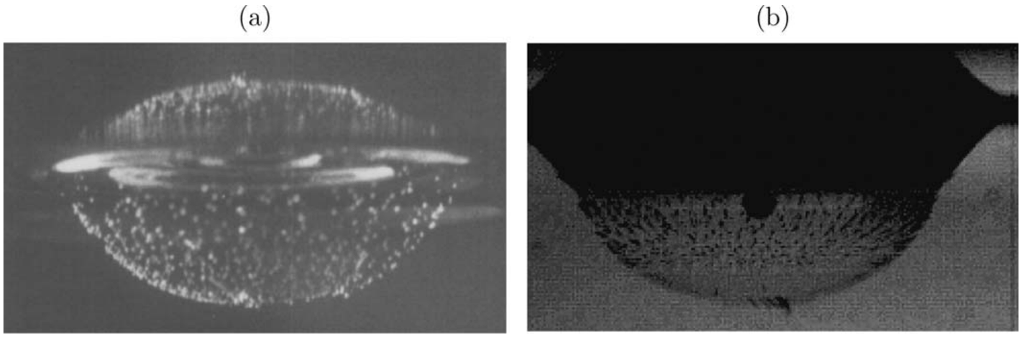

Figure 1. (a) Image taken from beneath the water surface of bubbles formed 10 ms after drop impact due to Sigler and Mesler,[5] (b) bubble formation pattern observed from beneath the water surface, due to the authors.

Note the similarity in the chandelier-like pattern in both images. The bubbles are black in (b) and white in (a) due to lighting differences. Formation of the large bubble in the center of (b) is observed intermittently. The width of each image is ≈5 mm.

size has not been established. To provide a better understanding of the progression of events that occurs during Mesler entrainment, a sequence of images is presented in Figure 2, obtained by the present authors. As in Figure 1, the view of the camera is from below the air/water interface, and hence the drop itself is never visible due to total internal reflection. The first image shows the moment when the drop just impacts the water surface, causing a slight dimpling of the water surface, which is the beginning of the crater. The next two images reveal the growth of the crater. Image 2(c) is the image just before bubbles are formed, and image 2(d) is the point where the bubbles are just formed. Subsequent images show how the crater reforms as the drop fluid merges with the bulk and how the bubbles are convected into the water bulk via a drop-formed vortex,[6,7] which is itself visualized by the small bubbles.

The initial studies of Mesler was motivated by his nucleate boiling research. Specifically, they were motivated by observations of augmented heat transfer during nucleate boiling in thin films[8] and observations that the rupture of a bubble at the air/water interface resulted in a significant increase in the number of nucleation sites at the solid/liquid interface in the area beneath the bubble rupture, which was perhaps the cause of the augmented boiling heat transfer in thin films.[9] Bergman and Mesler[2] showed that this occurs in thick liquid layers as well. The nucleation sites formed by a bubble rupture are referred to as secondary nucleation sites. Carroll and Mesler[1] hypothesized that the drops formed during a bubble rupture at the air/water interface subsequently impact that water surface where they entrained many small bubbles downward to the boiling surface which form the observed secondary nucleation sites. This hypothesis was the motivation of subsequent studies by Mesler and coworkers who sought to determine under what conditions a liquid drop impacting a water surface would result in bubble entrainment. Other researchers have also investigated the formation of many small bubbles by drop impacts, recognizing their significance, not only to nucleate boiling, but also in underwater noise generation,[10,11] gas exchange,[12–15] and other transport processes.

Esmailizadeh and Mesler[3] studied water drops ranging in diameter from 2.6 to 4.4 mm and dropped from heights as large as 30 mm. They observed the entrainment of hundreds of small bubbles and noted how the formation of a vortex due to the drop impact carries the bubbles a significant distance into the depth. They noted that the bubbles ranged in size from 50 to 100 μm, but that bubbles much smaller than these were probably present, but could not be resolved.

Sigler and Mesler,[5] using a 3 μs strobe pulse, imaged the events occurring just as bubbles are formed by an impacting drop. They noted that an air film is trapped between the falling drop and the bulk liquid surface, and imaged the breakdown of this air film into numerous small bubbles. One example of the images that they obtained is presented in Figure 1a. These authors postulated that the breakdown of the air sheet and formation of bubbles is due to the Rayleigh-Taylor instability. They frequently observed the chandelier pattern of bubble formation shown in Figure 1. They also sometimes observed the air sheet collapse in a fashion much like the rupturing of a balloon. This latter process produced a smaller number of larger bubbles and they postulated that it must be due to some other mechanism.

Oguz and Prosperetti studied mathematically the problem of a drop approaching a liquid bulk, incorporating surface tension, but not viscosity.[16] They obtained numerical solutions to their model and observed an alternative process by which many small bubbles may be obtained during a drop impact. Specifically they found that upon impact, capillary waves propagate outward from the impact site along both the bulk liquid surface and the lower surface of the drop. The crests of these waves line up, resulting in the formation of toroidal bubbles which would, presumably, break down subsequently into spherical bubbles. Oguz and Prosperetti suggest that this mechanism can explain the experimental results of Mesler and coworkers. Oguz and Prosperetti also suggested that the Rayleigh-Taylor mechanism proposed by Sigler and Mesler was unlikely the cause of the air film breakdown due to an insufficient rate of deceleration by the drop to sustain Rayleigh-Taylor breakup.

The chandelier-like structure seen in Figure 1 is not the only structure that has been observed where small bubbles are formed. For example, Thoroddsen et al.[17] used an ultra high speed video system to study the film of air trapped beneath an impacting drop and the subsequent bubble formation. They found several types of bubble formation events. However, with the exception of three images, these authors focused on drop impacts where a very small number of bubbles were formed. Similarly, Liow and Cole[18] obtained

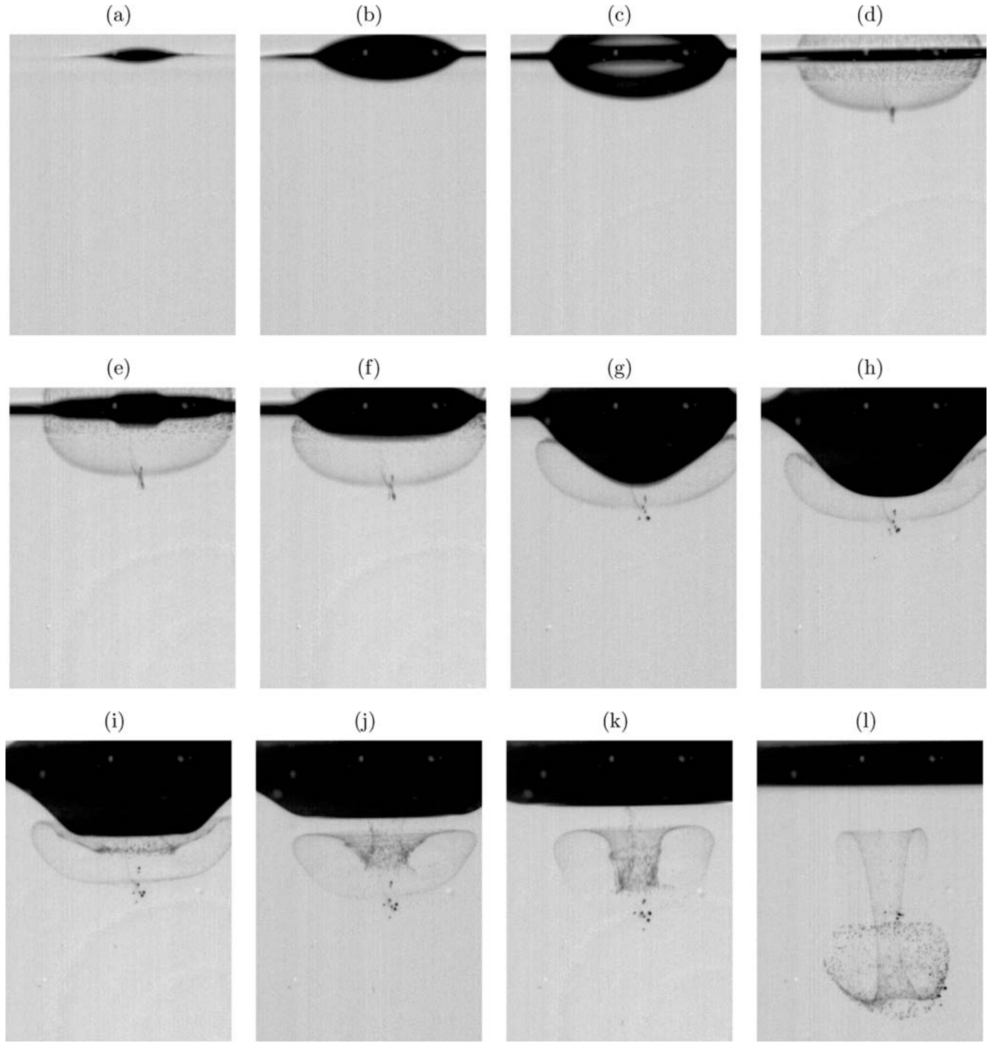

Figure 2. Sequence of images showing Mesler entrainment including the evolution of the crater, the formation of bubbles, and the subsequent convection of bubbles into the water bulk via the drop-formed vortex.

The time at which each image is taken relative to the first is: (a) 0, (b) 1.5, (c) 3, (d) 4, (e) 5, (f) 6, (g) 8.5, (h) 11, (i) 14, (j) 18, (k) 21.5, and (l) 52 ms. The camera is directed upward from below the water surface, so the drop is not visible due to total internal reflection. Images have been digitally processed to remove nonuniformities in the background and to enhance contrast. Note that, unlike Figure 1b, a large bubble is not formed.

images showing what they refer to as Mesler micro-bubbles, but these images show a very small number of bubbles and appear to be of a different mechanism from that seen in Figure 1. In this article, Mesler entrainment refers to bubble entrainment caused by a drop impact, which results in the nominally chandelier pattern of bubbles shown in Figure 1, and where the bubbles are small and numerous.

The parameters that are relevant to drop impact events are the liquid density ρ, the drop impact velocity V, surface tension σ, drop diameter d, the liquid absolute viscosity μ, and the gravitational acceleration g. The Buckingham pi theorem requires that three dimensionless groups describe this situation, and these are typically constructed in the form of the Weber, Froude and Capillary numbers defined as

$$We = \frac{\rho V^2 d}{\sigma} \tag{1}$$

$$Fr = \frac{V^2}{gd} \tag{2}$$

and

$$Ca = \frac{\mu V}{\sigma} \tag{3}$$

respectively. A convenient method for comparing images acquired by many authors is to plot the location where each image was obtained on Froude versus Weber number coordinates. This is presented in Figure 3, which shows the location of the images due to the aforementioned researchers, as well as that of the present study in $Fr-We$ space. The upper solid curve in the figure is the terminal velocity limit, where the terminal velocity was obtained from the relation due to Rogers[19] for drops smaller than 0.469 mm and the relation due to Atlas et al.[20] for drops greater than or equal to 0.469 mm in diameter. The space between the two slanted lines is the

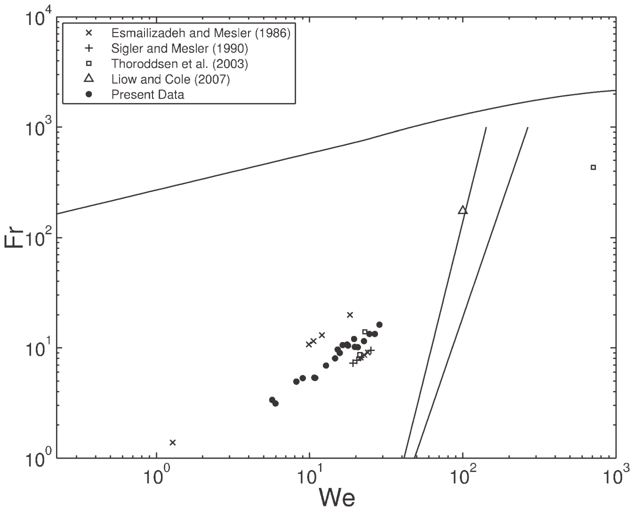

Figure 3. Plot showing the location of images obtained in the present study and in prior work in Froude versus Weber number space.

The upper curve is the terminal velocity limit. The region between the two diagonal line is the regular bubble entrainment region.

regular bubble entrainment regime, a region where a single bubble (order 1 mm in diameter) is formed for each drop impact.[21,22] For some of the data presented in Figure 3, the drop velocity, required to compute both We and Fr, was obtained from data on the drop release height, assuming acceleration of the drop without air drag. This plot shows that the data acquired herein falls just between that of Sigler and Mesler[5] and Esmailizadeh and Mesler.[3] It also shows that the data obtained by Liow and Cole[18] is quite distant from the regions explored by Mesler. The data presented for Thoroddsen et al.[17] correspond only to those images in his paper which show structures similar to those seen by Mesler, namely their Figures 7a, b and 8b.

A consistent observation made in virtually all of the experimental work done on Mesler entrainment concerns the effect of surface contamination. For example, Esmailizadeh and Mesler noted that when the container of water into which drops impacted was left overnight, very few drops were found to result in Mesler entrainment.[3] These authors hypothesized that surface contamination was the cause of this behavior. Sigler and Mesler noted that simply allowing freshly deionized water to sit in a laboratory environment for 15 minutes reduced the amount of small bubbles formed.[5] They attributed this to atmospheric dust. It is not surprising that surface contamination can affect the formation of bubbles due to drop impacts since indigenous surfactants can change surface tension, and surface tension is important in any drop and/or bubble process. For example, Saylor and Grizzard[7] demonstrated the effect that slightly varying surfactant concentrations can have on vortex rings formed by impacting drops, demonstrating the dependence of vortex penetration on the drop surface tension. Even small quantities of surfactant may significantly affect surface tension, elasticity and transport phenomena.[6,23,24] Moreover, even when water is cleaned to the point that a Wilhelmy plate apparatus reveals no surfactant contamination, surfactants may still exist on the water surface,[25] as revealed by infrared imagery.[26] Hence, when using "clean" water surfaces, one may simply be creating an environment where Mesler entrainment becomes highly variable due to varying degrees of contamination which occur at the water surface from run-to-run or even from drop-to-drop. This may be the cause of the lack of reproducibility in Mesler entrainment which was observed by, for example, Esmailizadeh and Mesler,[3] and Pumphrey and Elmore.[27]

Several open questions exist regarding the effect of the condition of the water surface on Mesler entrainment. First, Mesler's work seems to show that bubble formation decreases with the age of the water pool. If this is indeed the case, then it is possible that surfactants can stop Mesler entrainment altogether. Can Mesler entrainment exist in the presence of significant surfactant contamination? This is one of the questions we address in this article. Secondly, if Mesler entrainment does occur in the presence of surfactants, is the reproducibility improved? That is, can the reproducibility be improved by maintaining a constant surfactant contamination level? It seems that this should be possible by purposely contaminating the water surface with a large, fixed quantity of a known surfactant. By doing this, the relatively small amount of indigenous surfactant that might exist would play a minor role, thereby improving reproducibility. A related question is: if Mesler entrainment is still not made reproducible, can the occurrence of Mesler entrainment be quantified in a statistical sense? This is a second set of questions which this work addresses.

Mesler entrainment is very often observed in conjunction with a vortex, also caused by the drop impact.[1,3,27] It is not clear that Mesler entrainment and the formation of a vortex are necessarily related. That this is a possibility, however, should not be discounted. If indeed the two phenomena are related, then it should also be the case that the shape of the drop at impact would affect Mesler entrainment, since many experiments have shown that drop shape affects the formation of a vortex.[4,6,7,28–30] These experiments take advantage of the fact that a falling drop naturally oscillates between an oblate and prolate shape with the drop attaining a nominally spherical shape in between. By releasing a drop from progressively higher heights, shape oscillations result in a range of drop shapes at impact. We note that Esmailizadeh and Mesler[3] obtained images of bubble formation for drops falling from a sufficient range of heights to insure that one full period of drop oscillation occurred over that range. That is, their drops ranged in shape from prolate through oblate at impact. They note briefly that they did not see any change in bubble entrainment due to drop shape. However, it is possible that the authors were simply noting that they observed some amount of bubble entrainment for all drop shapes. It may be that a change in the probability of occurrence of Mesler entrainment occurred over that range, but that this was not noted. Hence, an open question which is addressed in this work is exactly how Mesler entrainment is affected by the drop shape. Specifically, we would like to determine the effect on Mesler entrainment of the axis ratio at impact, α, defined as

$$\alpha = \frac{d_v}{d_h} \tag{4}$$

where d_v is the maximum vertical extent of the drop and d_h is the maximum horizontal extent of the drop. If drop shape is indeed an important parameter, as we hypothesize, then α becomes a fourth dimensionless group controlling Mesler entrainment, in addition to the three defined above in Eqs. 1–3.

Existing work on Mesler entrainment has occasionally referred to the value of a Weber number or Froude number. However, we are unaware of a study which has attempted to determine a trend in some quantifiable aspect of Mesler entrainment in terms of a dimensionless group. Pumphrey and Elmore identified specific regions of impact velocity and drop diameter which resulted in one of four categories of entrainment, one of which was Mesler entrainment.[27] However, it was noted that in some types of entrainment it was difficult to isolate specific regions where the entrainment occurs. Specifically it was difficult to specify the impact parameters for which Mesler entrainment would occur, and the authors classified a large region of impact velocities and drop diameters where it was observed. Here we seek to correlate the frequency of occurrence of Mesler entrainment to the Weber number.

The Froude number is also expected to affect Mesler entrainment, however in the experiments presented here, the working fluid was fixed, and the drop diameter was nominally fixed (a small amount of data is presented for a second drop diameter—see the Discussion section). Hence, the Froude and Weber numbers are related by a multiplicative factor and an assessment of the individual role of We and Fr is not obtained here. This can be seen in Figure 3, which shows that the data obtained herein, when plotted on Fr versus We coordinates, falls on an (essentially) straight line. This is also true of the data obtained by Sigler and Mesler[5] and Esmailizadeh and Mesler.[3]

The capillary number is also expected to affect Mesler entrainment. Deng et al.[31] show how Ca affects bubble entrainment in the regular bubble entrainment region. The role of Ca in Mesler entrainment has not been addressed. However, since the primary fluid of interest in most Mesler entrainment applications is water of nominally constant viscosity, exploration of the role of Ca is left as future work.

In addition to its application to boiling heat transfer, Mesler entrainment is important to the study of gas exchange across the air/water interface of lakes, rivers and oceans. In these situations, small diameter, low impact velocity drops are created by the splashes of raindrops, bubbles popping at the surface, and from wave breaking events. Via Mesler entrainment, each of these small drops is capable of entraining many small bubbles. The small diameter of these bubbles results in a very low buoyancy force, enabling them to stay beneath the water surface for long periods of time, thereby transferring significant amounts of gas to the water. Understanding the conditions for Mesler entrainment is an important step toward developing models of the amount of gas entrained by these small bubbles in rivers, lakes, and oceans.

Experimental Method

The experimental setup used to conduct these experiments is presented in Figure 4. Drops were created using an 18 gauge hypodermic needle suspended over the reservoir surface. The tip of the needle was blunted to ensure uniform snap off and a vertical trajectory for each drop. Drop impacts were recorded for needle tip positions ranging from 1.25 to 3.5 cm above the water surface. A Cole-Palmer 74900 Series syringe pump provided flow to the needle through a flexible PVC tube.

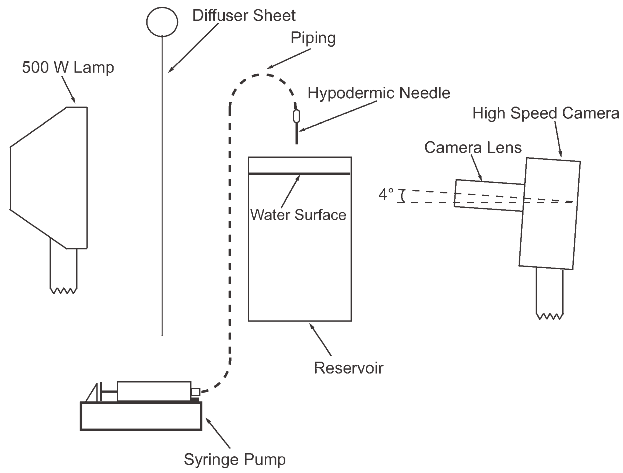

Figure 4. Apparatus used for recording drop impacts.

Drops impacted the surface of a water reservoir which was constructed of 1/4'' thick glass plates glued together with silicone rubber adhesive sealant providing an approximate length, width, and depth of 9.0 cm, 9.0 cm, and 17.8 cm, respectively. For all experiments, the drop fluid and the reservoir fluid consisted of a mixture of the soluble surfactant, Triton X-100 and doubly distilled water. The Triton X-100 concentration was 0.1 mg/L. The drop fluid was aspirated from the reservoir into the syringe just before the start of any experiment to ensure that both reservoir and drop had the same surfactant concentration. The critical micelle concentration (CMC) for Triton X-100 ranges from 0.22 to 0.24 mM, or 137 to 150 mg/L, and so the concentration used here is well below this CMC limit.[32]

Images of the drop impact and the subsurface formation of bubbles were obtained using a high speed camera (Fastech, Trouble Shooter) which recorded 8-bit grayscale images at a frame rate of 1000 fps for all experiments. The optical axis of the camera was located just below the water surface and at an upward viewing angle of approximately 4°. Lighting was provided from a 500 W lamp positioned behind a diffuser sheet consisting of translucent plastic. To prevent the lamp from heating the reservoir, a piece of cardboard was placed between the diffuser sheet and the tank to insulate the reservoir and the needle. A small opening was cut into the cardboard to allow sufficient light to pass to the camera. After each drop impacted the surface, the video was reviewed to assess the bubble entrainment scenario.

Surface tension was measured using a Sigma 703 tensiometer equipped with a Wilhelmy plate. The tensiometer was calibrated using a known weight. The Wilhelmy plate was thoroughly washed with methanol and doubly distilled water before use. In addition, the Wilhelmy plate was flamed to an orange color using a propane torch to remove any further contaminants. Although the drop fluid was obtained from the reservoir and hence had the same Triton X-100 concentration as the reservoir, there was some concern that the reservoir surface tension would change after drops impacted the surface. To address this issue, preliminary experiments were conducted where the surface tension was measured using the Wilhelmy plate during drop impacts. For these preliminary experiments, a drop rate of 6 drops/min was used. This drop rate resulted in an average decrease in the surface tension of the reservoir of 2.2 mN/m during the course of 1 hour. This average was obtained from four separate hour long experiments. The plots of surface tension versus time for these experiments are presented in Figure 5. The hour during which drop impacts occur is the region of linear decrease in surface tension seen in the center of each of the four time traces. No noticeable trend was observed between the entrainment scenario that occurred and the number of drop impacts that occurred. That is, Mesler entrainment was not observed with any greater or smaller frequency at the beginning or the end of one of these long sequences of drops. Hence, the change in surface tension seen in Figure 5 was deemed negligible with respect to the entrainment scenario. To stay consistent with these preliminary surface tension experiments, the same drop rate (6 drops/min) was used for the actual experiments. The syringe pump flow rate was adjusted, if necessary, throughout each hour long experiment to assure drops fell at this rate of 6 drops/min.

Because the Weber number used here is defined for the drop, and not for the reservoir surface, the appropriate value of the surface tension should be that of the drop. While the drop fluid and tank fluid had the same Triton X-100 concentration, one must consider the fact that the water surface on the tank was allowed to sit for 24 hours before running experiments (see later), while the surface of the water drops existed only for the time during which they formed on the needle tip (10 seconds for the 6 drops/min drop rate used here). Hence, the tank water had time for the surfactant concentration to reach an equilibrium concentration, while the same may not have been true for the drops. The evolution of the surface concentration of a soluble surfactant can be complicated during the drop formation process.[33] Moreover, it may be the case that the equilibrium concentration for the curved surface of a drop is not the same as for that of a flat surface. To address this, data obtained using the pendant drop data due to García-Blanco et al.[34] were used to correct the values of surface tension obtained here. Wilhelmy plate measurements were obtained on the reservoir for four different Triton X-100 concentrations: 0.01, 0.1, 1, and 10 mg/L. The difference between the values of σ obtained at each of these concentrations, and those obtained by García-Blanco et al.[34] were computed. On the average, the pendant drop measurements were larger than those obtained here by 13.8 mN/m. This value was added to our measurement of 54.38 mN/m to achieve the value of 68.18 mN/m at $c = 0.1$ mg/L which is used for σ herein. The value of water density, also needed in the Weber number was taken as $\rho = 997.3$ kg/m^3, based on the bulk water temperature.

Of the roughly 360 drops that fell during an experiment, only 30 sample drop impacts were recorded due to constraints in selecting and saving imagery. Images obtained from the high speed camera were used to measure the drop diameter, impact velocity, and the bubble entrainment scenario. Experiments were conducted over a range of drop heights (1.25–3.5 cm from the needle tip to the water surface in the reservoir) to achieve different impact velocities. Before each experiment began, video of a fine scaled rule was taken to provide a pixels/mm calibration for each experiment, enabling accurate measurement of drop diameter and velocity, both of which are needed in computation of the Weber number.

Care was taken in creating the Triton X-100 solution in the reservoir. For all experiments, a concentrated stock solution of 2.14 g/L of Triton X-100 was carefully mixed with known volumes of doubly distilled water to achieve the desired concentration of 0.1 mg/L. Care was taken to avoid creating bubbles while mixing the solution, since the surface of these bubbles can acquire and release surfactant over time. After mixing, the reservoir was covered with clear

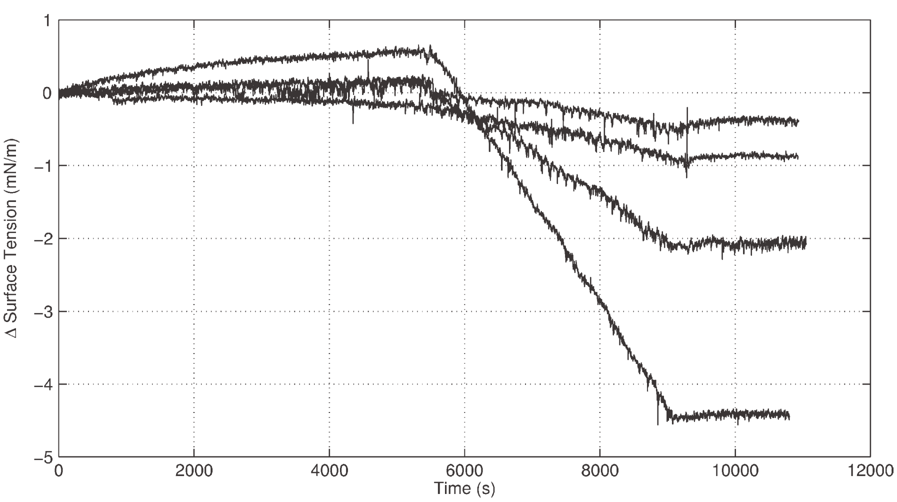

Figure 5. Change in surface tension of reservoir subjected to drop impacts at 6 drops/min for 1 hour for a Triton X-100 concentration of 0.1 mg/L.

The initial surface tension value is subtracted from each time trace plotted. The 1 hour period during which drop impacts occurred is the region of linear decrease in surface tension, which can be seen in each time trace.

plastic wrap to reduce contamination from the air. Preliminary experiments showed that the measured surface tension took approximately 4 hours to stabilize at a surfactant concentration of 0.1 mg/L; to assure a stable monolayer, the reservoir was allowed to sit for at least 24 hours before each experiment. The walls of the glass reservoir were thoroughly cleaned between experiments using methanol and doubly distilled water. The hypodermic needles, syringe, and piping were soaked in doubly distilled water for at least 24 hours before each experiment.

The bulk water temperature varied from a minimum of 23°C to a maximum of 26°C for the entire data set presented here. The bulk water temperature typically fell 0.4°C during the course of a single experiment. This decrease is most likely due to evaporative cooling which began when the plastic wrap was removed from the tank before each experiment. The air temperature varied from a minimum of 24°C to a maximum of 27°C and relative humidity varied from a minimum of 47% to a maximum of 57% over the course of the entire experimental program. The air temperature varied no more than 0.8°C and the relative humidity varied no more than 3% during the course of a single experiment.

Measurement of the drop velocity, diameter, and axis ratio required processing of the digital imagery to identify the boundaries of the drop in each frame. Once the images used to compute diameter and velocity were selected, the following image processing steps were taken to identify the drop boundary. First, the images were cropped to reduce processing time and simplify edge detection. Second, the Sobel edge operator[35] was applied to each image to enhance edges. Next, the contrast was enhanced with histogram equalization where the maximum and minimum intensities in the image were set to the limits for a 8-bit image and proportionally distributed over a specified number of gray levels, 64 in this work. A smoothing filter was then applied to reduce noise in the image. Finally, the Canny edge detection algorithm[36] was applied to the image with appropriate thresholds. These steps transformed each grayscale image into a binary one. Lighting varied slightly between experiments which necessitated adjustment of the thresholds used in the Canny algorithm. Processed images were saved and visually reviewed to assure that appropriate thresholds were applied, so that only the drop edge was left after processing of each image. Initial image identification and selection was done using ImageJ,[37] and all other image processing was done using Mathworks Matlab 2008b. The Canny algorithm was implemented using the version of the algorithm incorporated in the Matlab programming environment. An example of a raw and processed image is presented in Figure 6, showing a falling drop having a prolate shape.

Using the processed binary image, the velocity of each drop impact was calculated by measuring the distance traveled by the centroid of the drop in the 3 ms before the drop was obscured by the meniscus of the reservoir. At a frame rate of 1000 fps, and at the magnification and optical setup used, four frames showing a complete drop were captured before impact. A linear fit was applied to a plot of the position of the centroid of each of these four drop images versus time. The slope of the fit was taken as the instantaneous velocity before impact, and hence is an average obtained over 3 ms. The diameter of each drop was calculated assuming an

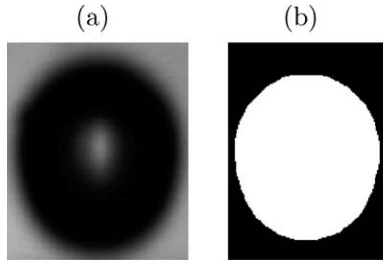

Figure 6. (a) Unprocessed drop image (cropped). (b) Processed drop image.

axisymmetric drop. That is, each row of pixels occupied by the drop was assumed to represent a cylindrical volume, and the sum of these volumes was computed to calculate a total volume for the drop. This volume was used to compute a diameter for an equivolume sphere. The average of the diameters obtained from each of the four images before impact was used as the drop diameter d in Eq. 1. To compute α, the largest column, d_v, and largest row, d_h, of pixels occupied by the drop in the last visible frame was measured and the vertical to horizontal axis ratio was calculated according to Eq. 4. The average diameter, obtained from all drops was $d = 2.80$ mm.

Results

In this work, a constant surface condition was approximated by using a constant concentration of the soluble surfactant Triton X-100 in both the drop fluid and the bulk fluid. This relatively constant condition has not been attained in prior work on Mesler entrainment. Despite this approach, Mesler entrainment did not occur reproducibly for drop impacts of nominally identical conditions. Specifically, three different impact outcomes were observed: (1) Mesler entrainment, (2) floating drops, or (3) some other event. Most drop impacts resulted in either Mesler entrainment, or a floating drop. Floating drops (sometimes referred to as bouncing drops) are drops that do not immediately coalesce with the water surface, sometimes bouncing several times before merging with the bulk water.[38] Occasionally, some other form of bubble entrainment was observed, such as the formation of a small number of relatively large bubbles, and this is referred to as "other," herein. Sample images showing the impact crater and the resulting bubble formation event (if any) for each of these three scenarios are shown in Figure 7.

To quantify Mesler entrainment, drops were binned according to Weber number and the frequency of occurrence was computed for each of the following scenarios: Mesler entrainment, floating drops, and Mesler entrainment or floating drops. This frequency of occurrence f for a specific bin was simply the number of drops in that bin which exhibited that behavior (e.g., Mesler entrainment), divided by the total number of drops in that bin. Figure 8 presents f for these three scenarios plotted against We. Each point on the plot represents a bin for that particular Weber number. It is noted that although there are small variations in the drop diameter from drop-to-drop in the data presented in Figure 8 which affect We, the Weber number is primarily varied by changing the drop release height, and thereby the drop impact velocity. The total number of recorded drops was 520 and

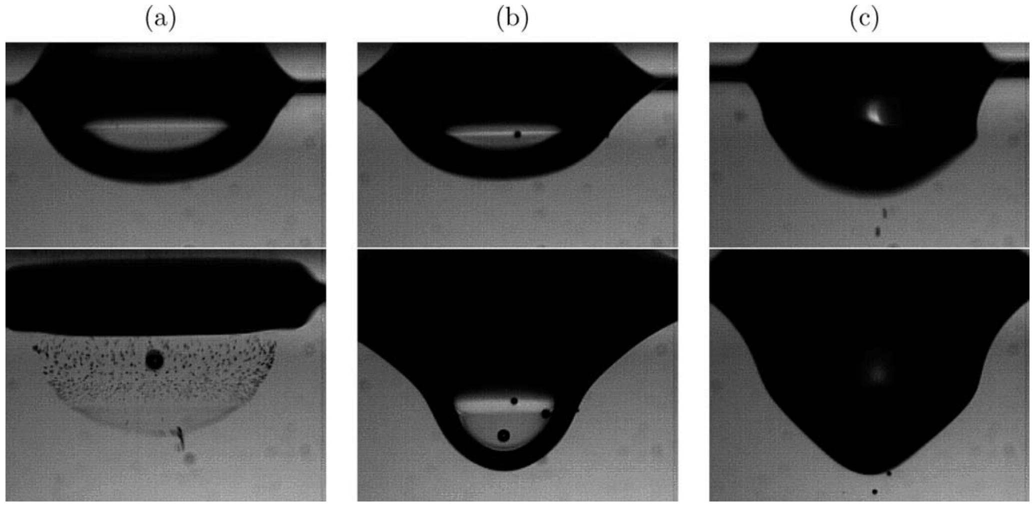

Figure 7. Three different impact scenarios observed: (a) Mesler entrainment, (b) floating or bouncing drop, and (c) other entrainment.

The upper row of images shows the crater geometry. The lower row of images shows the resulting bubble formation scenario (if any). Note that in (b), bubbles from a prior drop impact are visible. For all six images, the width is 6.1 mm. The height is 3.9 mm in the upper row of images and 4.9 mm in the lower row of images.

bins possessing fewer than 10 drops were not plotted. All three plots reveal a dependency on Weber number. In Figure 8a, two peaks appear where Mesler entrainment can be observed. This multiple peak behavior is typical of phenomena sensitive to drop oscillations as observed, for example, in studies of drop impacts and vortex ring penetration.[4,6,7] This is discussed further below.

The criterion used herein to ascertain the existence of Mesler entrainment was necessarily subjective. Specifically, drop impacts that had the chandelier-like appearance of the images presented in Figure 1 were defined as exhibiting Mesler entrainment. This criteria was fairly straightforward to implement, however there was a small degree of ambiguity for larger Weber numbers. This is illustrated in Figure 9, where the bubble formation event of two drops are shown, one at $We = 14$, and one at $We = 21$. For the $We = 14$ case shown in Figures 9a–d, a chandelier pattern of bubbles is clearly formed, and the large number of small bubbles is transported downward in a drop-induced vortex. For the $We = 21$ case it appears that a similar, but smaller chandelier structure is present, however resolution limits prohibit us from determining if the pattern is exactly the same as for the smaller Weber number situation. The bubbles are smaller in this case, and are transferred into the bulk by the vortex, as for the $We = 21$ case. We do not think there is a fundamentally different bubble formation mechanism at these two peaks. Both peaks exhibit similar qualities such as numerous bubbles, a collapsing air film and what appears to be the chandelier pattern.

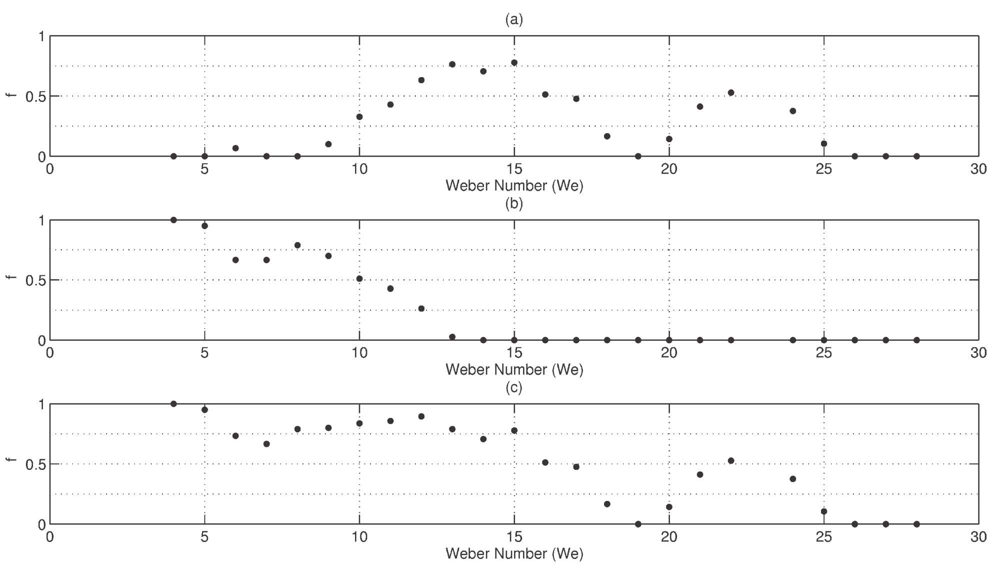

Figure 8. Plots of frequency of occurrence *f* of impact events versus Weber number *We* for (a) Mesler entrainment, (b) floating drops, and (c) Mesler entrainment or floating drops.

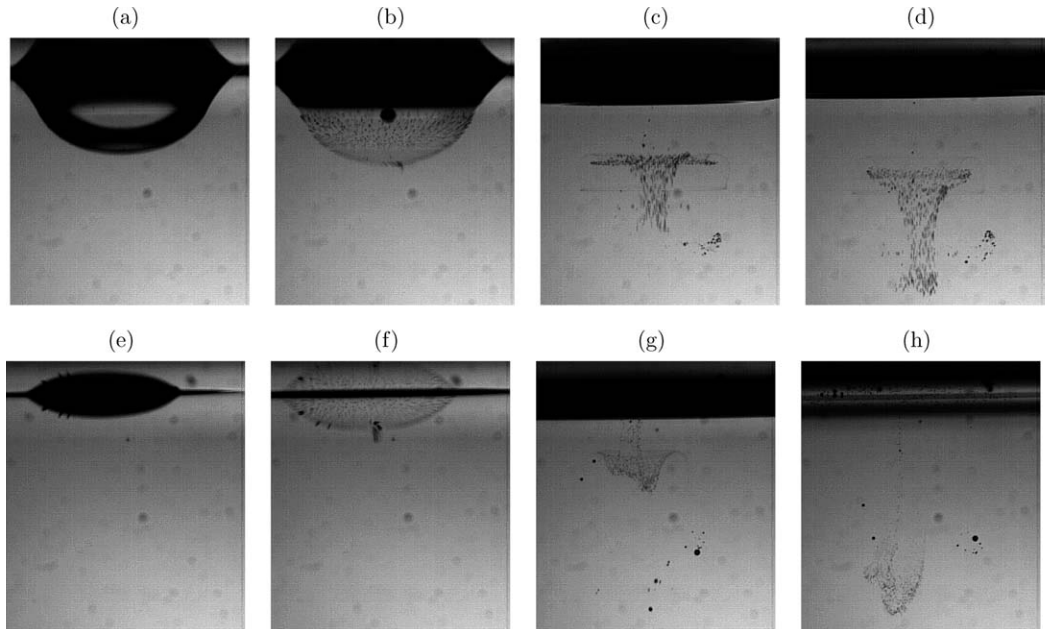

Figure 9. Images showing Mesler entrainment at (a–d) low Weber number *We* = 14, and (e–h) high Weber number *We* = 21.

For the upper row, times after impact are (a) 7, (b) 8, (c) 23, and (d) 30 ms, respectively. For the lower row, times after impact are (e) 2, (f) 3, (g) 44, and (h) 91 ms, respectively. For each image the width is 6.1 mm and the height is 6.9 mm.

As noted earlier, the bubbles formed by the drop impacts shown in Figure 9 are transported downward by a vortex. Some of the bubbles stay with the vortex, and some are left behind in a trail. Occasionally drop impacts that resulted in the formation of the chandelier pattern of bubbles was not accompanied by the vortex and trail structures. Esmailizadeh and Mesler made a similar observation.[3]

As noted earlier, falling drops undergo shape mode oscillations, varying from a prolate shape to an oblate shape, and achieving a spherical shape between these two extremes. This was the case for the drops studied here. To determine any dependence of Mesler entrainment or floating drops on drop shape, the frequency of occurrence f of both scenarios is plotted against α in Figure 10. Unlike the dependence of floating drops on We shown in Figure 8b, f for floating drops shows no dependence on α, as Figure 10b reveals. A finite number of Mesler entrainment events are observed for all α (see Figure 10a). The likelihood of observing Mesler entrainment is highest at $\alpha = 1$, that is for spherical drops. In Figure 10c, the data of Figure 10a are replotted, but only for

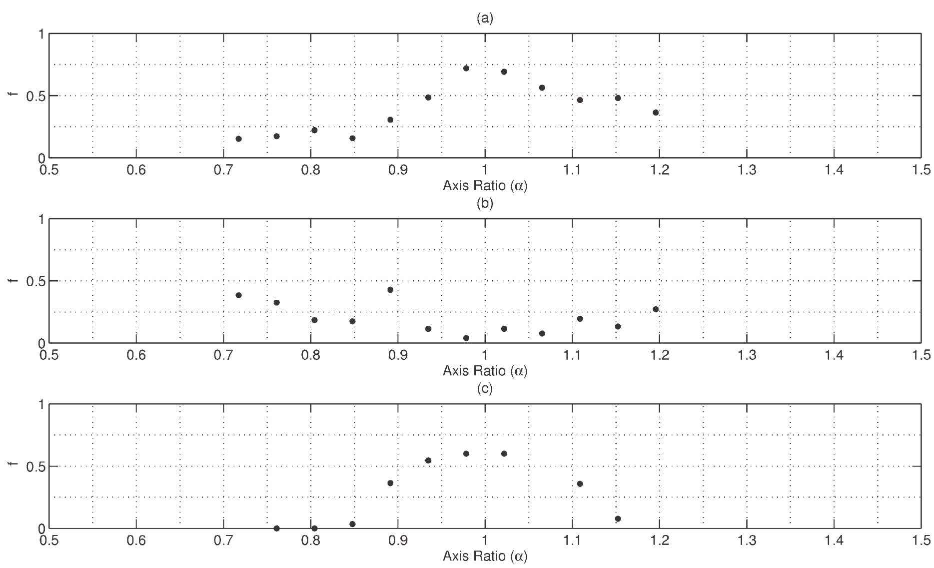

Figure 10. Plots of frequency of occurrence *f* of impact events versus axis ratio, α for (a) Mesler entrainment, and (b) floating drops, (c) plot of *f* for Mesler entrainment versus α using only data where *We* > 19.

those drops where $We > 19$. The same peak is observed at $\alpha \approx 1$; however, at very large or very small axis ratios Mesler entrainment is not observed at all. This suggests that as the Weber number becomes sufficiently high, the effect of α on Mesler entrainment becomes more important. Because floating drops reveal no sensitivity to α, we conclude that the occurrence of floating drops depends only on We for constant viscosity conditions.

Figures 8 and 10 suggest that both We and α affect the occurrence of Mesler entrainment. However, plotting We versus α reveals that they are not independent, as shown in Figure 11. This behavior is expected since the only experimental parameter that changed significantly in these experiments is the drop height; the same needles for creating drops were used in all experiments presented heretofore. Therefore, drops underwent the same snap off dynamics and the only factor controlling α at impact was the height of the drop at snap off. The scatter observed in Figure 11 can be attributed to imperfections among needles and variations in the setup as a result of cleaning and changing needles.

The peaks and troughs in Figure 11 align closely with peaks and troughs of Figure 8a which makes it difficult to discern whether the behavior seen in Figure 8a is due to We, α, or both. This issue is resolved in the next section.

Discussion

Triton X-100 was used in this work in an attempt to stabilize the surface tension of the water surface. This approach largely succeeded. As noted in the Experimental Method section, at a drop rate of 6 drops/min, the surface tension changed by only 2.2 mN/m over the course of 1 hour. Hence, it seems that this approach reduced the effect of any adventitious surfactants on the water surface tension. Despite this approach, however, Mesler entrainment still did not occur reproducibly for drops falling under nominally identical conditions. It is unclear whether this is because the precautions that we took were insufficient to keep the water surface in a stable state (e.g., perhaps the 2.2 mN/m change in surface tension over the course of 1 hour is still much too large to allow Mesler entrainment to occur reproducibly), or whether Mesler entrainment is an inherently irreproducible process. It is possible that our drop rate was too high to allow the monolayer to reform on the bulk water surface in between drop impacts, and that this might cause the irreproducibility. However, preliminary experiments conducted at a drop rate of 0.5 drops/min showed no improvement in reproducibility of the data and indeed decreased the reproducibility slightly. It is also possible that the complexities of the evolution of the surfactant concentration on the surface of the drop during it's formation process may contribute to the lack of irreproducibility. Further experiments are needed to ascertain this, perhaps using a working fluid that is not as susceptible as water to surfactant contamination.

While Mesler entrainment was not found to occur reproducibly, its frequency of occurrence was found to be well correlated to We and α. The frequency of occurrence of floating drops also was well correlated to We, but not to α. The frequency of occurrence of floating drops was shown to decrease almost monotonically from $f = 1$ at $We = 4$ to $f = 0$ at $We = 14$, as seen in Figure 8. Indeed, a portion of this region shows practically linear behavior. The frequency of occurrence of Mesler entrainment showed a periodic variation with We, with peaks at $We = 14$ and 22.

In addition to the effect of We on Mesler entrainment, the data, as presented in Figure 10 show the effect of drop shape, as quantified by α. Specifically, when all of the data are included, the results show that the frequency of occurrence of Mesler entrainment is maximized when the drop is spherical ($\alpha = 1$), and that f decreases as α deviates from unity. As Figure 10 shows, the decrease in frequency of occurrence of Mesler entrainment with increasing/decreasing α is asymmetric and noisy. However, if only the data for $We > 19$ is utilized, the plot of frequency of occurrence versus Mesler entrainment becomes smoother and much more symmetric.

Figures 8 and 10 suggest that the frequency of occurrence of Mesler entrainment is affected by both We and α. However, Figure 11 shows that a strong correlation exists between α and We for this data; thus it is not completely clear that We and α independently affect the occurrence of

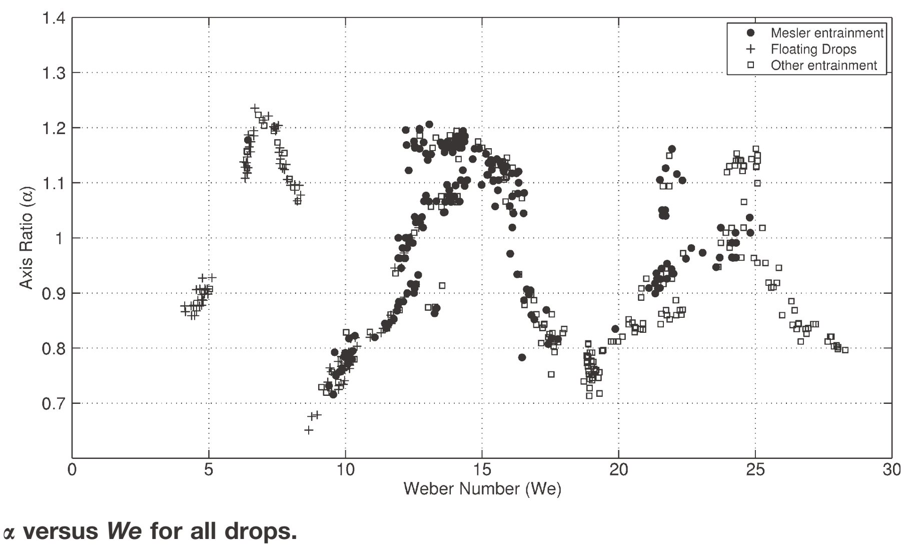

Figure 11. Plot of α versus *We* for all drops.

Note that, unlike Figures 8 and 10, the data are not binned in this plot.

Mesler entrainment. Figure 10c suggests that α and We do both play a role by demonstrating that the occurrence of Mesler entrainment at the extreme axis ratios decreases significantly for sufficiently large We. Nevertheless, to assure that both α and We are factors in the occurrence of Mesler entrainment, a second set of experiments was conducted using the same procedure as that heretofore except for the use of different needles to produce drops having a different drop diameter. Specifically, disposable pipet tips were chosen to produce slightly larger drops. By changing the drop diameter, at a fixed value of We, a different value of α can be attained at impact, decoupling We from α. Why this is so is now shown.

The resonant frequency of a spherical drop is

$$f_{\mathrm{d}} = \sqrt{\frac{2n(n-1)(n+2)\sigma}{\pi^2 \rho d^3}} \tag{5}$$

where n is the harmonic.[39,40] For the fundamental, $n = 2$ giving

$$f_{\mathrm{d}} = \frac{4}{\pi}\sqrt{\frac{\sigma}{\rho d^3}} \tag{6}$$

The number of oscillations that a drop undergoes before impact with the water surface is

$$n_{\mathrm{osc}} = f_{\mathrm{d}} t_{\mathrm{f}} \tag{7}$$

where t_{f} is the drop fall time which (assuming no air resistance for the sake of this demonstration) is

$$t_{\mathrm{f}} = \sqrt{\frac{2h}{g}} \tag{8}$$

and the impact velocity is

$$V = \sqrt{2gh} \tag{9}$$

where h is the fall height. Substituting Eq. 9 into Eq. 1 for a fixed Weber number, We_0, gives

$$h = \frac{We_0 \sigma}{2g\rho d} \tag{10}$$

Substituting Eqs. 6, 8, and 10 into Eq. 7 gives

$$n_{\mathrm{osc}} = \frac{4\sigma}{\pi \rho g d^2}\sqrt{We_0} \tag{11}$$

Because the fluid properties remain fixed in this work, the ratio of n_{osc} for two different drop diameters (again, for fixed Weber number, We_0) is

$$\frac{n_{\mathrm{osc}}(d_2)}{n_{\mathrm{osc}}(d_1)} = \left(\frac{d_1}{d_2}\right)^2 \tag{12}$$

As noted in the Experimental Method section, the nominal drop diameter was $d_1 = 2.80$ mm. In these additional experiments, the diameter was increased to $d_2 = 3.07$ mm, giving a ratio for the number of oscillations of 0.83. For a Weber number, say, of $We_0 = 15$, this gives $n_{\mathrm{osc}}(d_1) = 4.38$ and $n_{\mathrm{osc}}(d_2) = 3.64$. Hence, the drops for these experiments will impact the water surface at a different axis ratio than drops from the original experiments, at the same We. That is, an oscillation phase shift existed between these drops and the previous ones. Of course there will be a small error in the above computations since air drag has been neglected, however there will still be a phase shift in the shape of the two sets of data in terms of the shape of the drop at impact, for a given Weber number.

The experiments were conducted for a range of We where Mesler entrainment did not occur frequently in previous trials, specifically for $We = 19$. Figure 12a presents a plot of f for Mesler entrainment versus We with the new data superimposed over the earlier results. The new data lies above and to the left of the older data. The difference between the new data and old data shows that α has an effect on the occurrence of Mesler

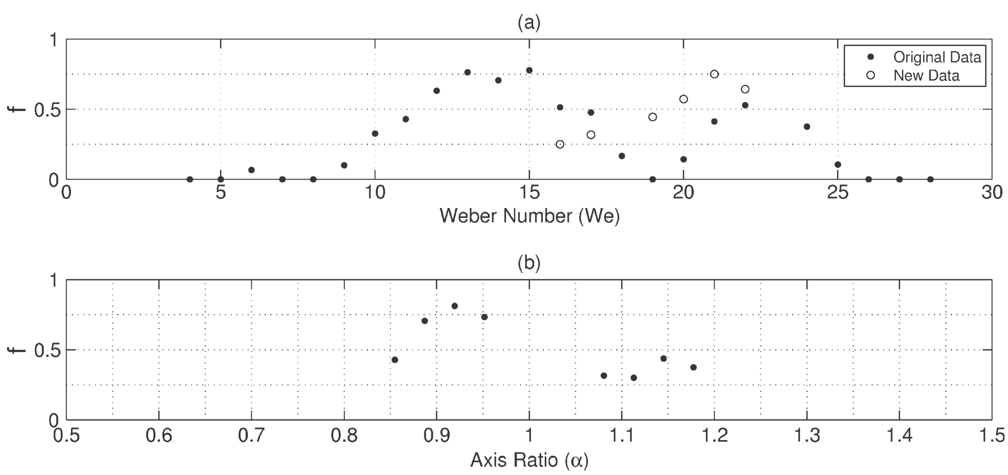

Figure 12. (a) Frequency of occurrence *f* of Mesler entrainment versus Weber number for drop impacts with new pipet tip superimposed over previous data. (b) Frequency of occurrence of Mesler entrainment versus α for new drop impacts.

entrainment, independent of We, since Mesler entrainment occurred with a different frequency simply because of a different α at impact. Figure 12b presents f for Mesler entrainment versus α for the new drop impacts. This graph peaks at $\alpha = 0.925$ instead of $\alpha = 1$ as seen in previous results. This is believed to be a result of too few samples collected.

Testik[41] studied the main outcome regimes for binary water drop collisions (i.e., bounce, coalescence, and breakup), and developed a physics-based theoretical $We - p$ diagram for the drop collision outcomes, where p is the diameter ratio of the smaller to the larger of the colliding drops. The impact of a drop with a water reservoir which is investigated here can be considered as the asymptotic case of binary drop collisions, i.e., $p \rightarrow 0$. For this asymptotic condition, Testik predicts the occurrence of floating drops for $We \leq 6$, and coalescing (i.e., entrainment) drops for $We > 6$. Figure 8b shows that floating drops occur exclusively when $We < 5$, showing reasonable agreement with the work of Testik, especially given the spacing in We in this work. Furthermore, the results in Figure 10b shows no sensitivity of floating drops to α, indicating that We is the only parameter affecting the occurrence of floating drops, also in agreement with Testik. However, as shown in Figure 8, for $4 < We < 14$ f for floating drops decreases with We, while f for Mesler entrainment increases with We. In Testik, a discrete transition from floating drops to coalescence is predicted. This difference may be attributed to several factors including the finite elasticity in the present work due to the use of surfactants, as well as factors that were not considered in Testik such as viscosity.

The occurrence of floating drops depends solely on We in this work. For these experiments, where σ and d were (essentially) unvarying, We is a measure of the kinetic energy of the drop. Since images like those presented in Figure 7 suggest that the initial geometry of the crater is essentially the same for situations resulting in Mesler entrainment and floating drops, it seems that the transition from purely floating drops to only Mesler entrainment with increasing We is a result of increasing drop kinetic energy. That is, without sufficient kinetic energy, the drops bounce away, while with sufficient kinetic energy they do not, and tend to result in Mesler entrainment.

One of the motivating questions of this work was whether surfactants can completely eliminate Mesler entrainment. Herein, Triton X-100 at a concentration of 0.1 mg/L was employed in both the bulk and drop fluid, and Mesler entrainment was not eliminated. Indeed, as Figure 8 shows, for intermediate We, Mesler entrainment was observed for over 75% of the drops.

Another phenomenon that can occur when a drop strikes a flat water interface is the formation of a vortex which penetrates into the water bulk. Much research has been conducted on this topic that suggests that the drop shape at impact determines the velocity and penetration depth of the resulting vortex. The sensitivity of Mesler entrainment to drop shape (α) observed here naturally leads to the question of whether the formation of a highly penetrating vortex and Mesler entrainment are somehow related, or at least occur under similar conditions. This is a difficult question to answer since, as pointed out by Saylor and Grizzard,[7] exactly what shape results in maximal vortex penetration is unclear, with some authors observing maximal vortex penetration when at impact a drop has a spherical shape and is in the process of changing from an oblate to a prolate shape,[29,30] while other authors found that vortex penetration was deepest when the drop is prolate at impact.[4] The experiments of Saylor and Grizzard[7] suggest that drop shape does have a strong influence on vortex penetration, but that the shape at which maximal vortex penetration occurs is itself dependent on the surface tension of the drop. Saylor and Grizzard used Triton X-100 in their experiments, and in one of their runs, the bulk fluid had a concentration $c = 0.125$ mg/L, close to the value of $c = 0.1$ mg/L used in the present study. Saylor and Grizzard[7] considered two Triton X-100 drop concentrations of 0 and 4.0 mg/L. Since these concentrations bracket the drop concentration used in the present work, it is logical to expect the value of We at which a peak in Mesler entrainment occurs herein to fall between the values of We at which maximal vortex penetration occurred in the two cases of Saylor and Grizzard,[7] if the two phenomena are enhanced by the same conditions. Saylor and Grizzard recorded peaks in vortex penetration at $We = 25.3$ and 39.8 for the $c = 0$ mg/L drops and at $We = 28.7$ and 47.3 for the $c = 4.0$ mg/L drops. The smallest of the peaks for both of those cases occurs at Weber numbers significantly above the largest peak for Mesler entrainment in the present study, suggesting that conditions which favor vortex penetration need not favor Mesler entrainment.

Conclusion

Experiments were performed to reveal the effect of Weber number and drop axis ratio on the occurrence of Mesler entrainment. The experiments were conducted using a constant surfactant concentration in an attempt to improve repeatability. Drop parameters were measured using high speed imagery. For Weber numbers greater than 8 and less than 26, Mesler entrainment was observed and peaks in Mesler entrainment occurrence were observed at $We = 14$ and 22. Mesler entrainment was also observed more frequently within this range of Weber numbers for axis ratios approximately equal to one. Drops of a prolate or oblate shape showed significantly less frequent Mesler entrainment especially as the Weber number became larger. The effect of axis ratio on Mesler entrainment became larger as the Weber number became larger. The presence of a surfactant does not seem to eliminate Mesler entrainment, at least for the concentration of the soluble surfactant Triton X-100 used here. However, the presence of a surfactant did not stabilize the situation in terms of allowing Mesler entrainment to occur with a high level of repeatability.

Acknowledgments

The authors gratefully acknowledge the assistance of Ms. Aynsley Zollinger in conducting preliminary experiments.

Literature Cited

1. Carroll K, Mesler R. Part II: bubble entrainment by drop-formed vortex rings. *AIChE J*. 1981;27:853–855.
2. Bergman T, Mesler R. Bubble nucleation studies. Part I: formation of bubble nuclei in superheated water by bursting bubbles. *AIChE J*. 1981;27:851–853.
3. Esmailizadeh L, Mesler R. Bubble entrainment with drops. *J Colloid Interface Sci*. 1986;110:561–574.

4. Rodriguez F, Mesler R. The penetration of drop-formed vortex rings into pools of liquid. *J Colloid Interface Sci.* 1988;121:121–129.
5. Sigler J, Mesler R. The behavior of the gas film formed upon drop impact with a liquid surface. *J Colloid Interface Sci.* 1990;134:459–474.
6. Saylor JR, Grizzard NK. The effect of surfactant monolayers on vortex rings formed from an impacting water drop. *Phys Fluids.* 2003;15:2852–2863.
7. Saylor JR, Grizzard NK. The optimal drop shape for vortices generated by drop impacts: the effect of surfactants on the drop surface. *Exp Fluids.* 2004;36:783–790.
8. Mesler R. A mechanism supported by extensive experimental evidence to explain high heat fluxes observed during nucleate boiling. *AIChE J.* 1976;22:246–252.
9. Mesler R, Mailen G. Nuclear boiling in thin liquid films. *AIChE J.* 1977;23:954–957.
10. Oğuz HN, Prosperetti A. Numerical calculations of the underwater noise of rain. *J Fluid Mech.* 1991;228:417–442.
11. Prosperetti A, Oğuz HN. The impact of drops on liquid surfaces and the underwater noise of rain. *Annu Rev Fluid Mech.* 1993;25:577–602.
12. Woolf DK. Bubbles and the air-sea transfer velocity of gases. *Atmos Ocean.* 1993;31:517–540.
13. Asher WE, Karle LM, Higgins BJ, Farley PJ, Monahan EC, Leifer IS. The influence of bubble plumes on air-seawater gas transfer velocities. *J Geophys Res.* 1996;101:12027–12041.
14. Woolf DK, Leifer IS, Nightingale PD, Rhee TS, Bowyer P, Caulliez G, de Leeuw G, Larsen SE, Liddicoat M, Baker J, Andreae MO. Modelling of bubble-mediated gas transfer: Fundamental principles and a laboratory test. *J Marine Systems.* 2007;66:71–91.
15. Wanninkhof R, Asher WE, Ho DT, Sweeney C, McGillis WR. Advances in quantifying air-sea gas exchange and environmental forcing. *Annu Rev Mar Sci.* 2009;1:213–244.
16. Oğuz HN, Prosperetti A. Surface-tension effects in the contact of liquid surfaces. *J Fluid Mech.* 1989;203:149–171.
17. Thoroddsen ST, Etoh TG, Takehara K. Air entrapment under an impacting drop. *J Fluid Mech.* 2003;478:125–134.
18. Liow JL, Cole DE. Bubble entrapment mechanisms during the impact of a water drop. Presented at the 16th Australasian Fluid Mechanics Conference, Gold Coast, Australia, 2007 866–869.
19. Rogers RR. Raindrop collision rates. *J Atmos Sci.* 1989;46:2469–2472.
20. Atlas D, Srivastava RC, Sekhon RS. Doppler radar characteristics of precipitation at vertical incidence. *Rev Geophys Space Phys.* 1973;2:1–35.
21. Oğuz HN, Prosperetti A. Bubble entrainment by the impact of drops on liquid surfaces. *J Fluid Mech.* 1990;219:143–179.
22. Pumphrey HC, Crum LA. Underwater sound produced by individual drop impacts and rainfall. *J Acoust Soc Am.* 1989;85:1518–1526.
23. Saylor JR, Handler RA. Capillary wave gas exchange in the presence of surfactants. *Exp Fluids.* 1999;27:332–338.
24. Lee RJ, Saylor JR. The effect of a surfactant monolayer on oxygen transfer across an air/water interface during mixed convection. *Int J Heat Mass Trans.* 2010;53:3405–3413.
25. Albrecht O. Commonly used criteria for checking the cleanliness of Langmuir-Blodgett equipment and spreading solvents are not sufficient. *Thin Solid Films.* 1989;178:563–565.
26. Saylor JR. Determining liquid substrate cleanliness using infrared imaging. *Rev Sci Instrum.* 2001;72:4408–4414.
27. Pumphrey HC, Elmore PA. The entrainment of bubbles by drop impacts. *J Fluid Mech.* 1990;220:539–567.
28. Thomson JJ, Newall HF. On the formation of vortex rings by drops falling into liquids and some allied phenomena. *Proc R Soc Lond.* 1885;39:417–436.
29. Chapman DS, Critchlow PR. Formation of vortex rings from falling drops. *J Fluid Mech.* 1967;29:177–185.
30. Durst F. Penetration length and diameter development of vortex rings generated by impacting water drops. *Exp Fluids.* 1996;21:110–117.
31. Deng Q, Anilkumar AV, Wang TG. The role of viscosity and surface tension in bubble entrapment during drop impact onto a deep liquid pool. *J Fluid Mech.* 2007;578:119–138.
32. Hait SK, Moulik SP. Determination of critical micelle concentration (CMC) of nonionic surfactants by donor-acceptor interaction with iodine and correlation of CMC with hydrophile-lipophile balance and other parameters of the surfactants. *J Surf Detergents.* 2001;4:303–309.
33. Jin F, Stebe KJ. The effects of a diffusion controlled surfactant on a viscous drop injected into a viscous medium. *Phys Fluids.* 2007;19:112103.
34. García-Blanco F, Elorza MA, Arias C, Elorza B, Gomez-Escalonilla I, Civera C, Galera-Gomez PA. Interactions of 2,2,2-trifluoroethanol with aqueous micelles of Triton X-100. *J Colloid Interface Sci.* 2009;330:163–169.
35. Sobel IE. *Camera Models and Machine Perception*. Stanford, CA: Stanford University Press, 1970.
36. Canny J. A computational approach to edge detection. *IEEE Trans Pattern Anal Mach Intell.* 1986;8:679–698.
37. Rasband WS. Image J National Institutes of Health, Bethesda, Maryland, 1997–2009.
38. Walker J. Drops of liquid can be made to float on liquid—what enables them to do so. *Sci Am.* 1978;238:151–158.
39. Rayleigh Lord. On the capillary phenomena of jets. *Proc R Soc Lond.* 1879;29:71–97.
40. Landau LD, Lifshitz EM. *Fluid Mechanics. Course of Theoretical Physics*, Vol. 6. Oxford, UK: Pergamon Press, 1989.
41. Testik FY. Outcome regimes of binary raindrop collisions. *Atmos Res.* 2009;94:389–399.

Manuscript received July 1, 2010, and revision received Dec. 29, 2010.